Electrochemical Conversion of CO₂ to Syngas with Controllable CO/H₂ Ratios over Co and Ni Single-Atom Catalysts

Qun He⁺, Daobin Liu⁺, Ji Hoon Lee⁺, Yumeng Liu, Zhenhua Xie, Sooyeon Hwang,
Shyam Kattel,* Li Song,* and Jingguang G. Chen*

Abstract: *The electrochemical CO₂ reduction reaction (CO₂RR) to yield synthesis gas (syngas, CO and H₂) has been considered as a promising method to realize the net reduction in CO₂ emission. However, it is challenging to balance the CO₂RR activity and the CO/H₂ ratio. To address this issue, nitrogen-doped carbon supported single-atom catalysts are designed as electrocatalysts to produce syngas from CO₂RR. While Co and Ni single-atom catalysts are selective in producing H₂ and CO, respectively, electrocatalysts containing both Co and Ni show a high syngas evolution (total current $> 74\ mA\,cm^{-2}$) with CO/H₂ ratios (0.23–2.26) that are suitable for typical downstream thermochemical reactions. Density functional theory calculations provide insights into the key intermediates on Co and Ni single-atom configurations for the H₂ and CO evolution. The results present a useful case on how non-precious transition metal species can maintain high CO₂RR activity with tunable CO/H₂ ratios.*

The extensive consumption of fossil fuels has caused the ever-increasing CO₂ emission, thereby bringing unparalleled and urgent climate problems.[1] In this regard, many emerging technologies such as sequestration, chemical fixation, and electro/photochemical reduction have been proposed to suppress CO₂ release.[2] Among these technologies, the electrochemical CO₂ reduction reaction (CO₂RR) has been regarded as a potential route to achieve a net reduction of CO₂ and produce value-added chemicals and fuels when integrated with renewable energy resources.[3] To date, many efforts for the exploration of efficient CO₂RR electrocatalysts have been made and various reaction pathways toward not only C₁ products but also multi-carbon products (such as C₂H₄, C₂H₅OH, etc.) are well-established. Among the possible products, the production of CO is considered as an attractive approach because CO can be readily utilized as a feedstock for value-added chemicals and fuels through the existing downstream thermochemical reactions.[3b, 4] For these reasons, gold (Au), silver (Ag), zinc (Zn), and palladium (Pd) have been extensively investigated for CO production.[5]

However, most of the electrocatalysts so far have offered a limited versatility for such a hybrid electro/thermocatalytic process due to the following two reasons. First, their product ratio might not be suitable for the typical syngas (CO/H₂) utilization in the thermocatalytic synthesis as a result of suppressing the hydrogen evolution reaction (HER), which is a major competing reaction of CO₂RR. Second, a high yield production of CO from the dissolved CO₂ remains challenging. Therefore, it is desirable to develop electrocatalysts that can deliver the suitable CO/H₂ ratio with high syngas yield.

In this study, we investigated the earth-abundant *3d* transition metal-embedded N-doped carbons (denoted as TM-NC with TM = Co and/or Ni) as CO₂RR electrocatalysts. Through X-ray diffraction (XRD), X-ray absorption fine structure (XAFS), and high-resolution electron microscopy analyses, it was confirmed that single TM atom could be effectively anchored into N-doped carbon supports due to the favorable TM−N bond formation, thus enabling distinct CO₂RR behavior from the typical bulk counterparts in terms of the ratio and yield of CO/H₂. In such a single-atom configuration, Ni-NC exhibited an almost exclusive activity to CO evolution ($>56\ mA\,cm^{-2}$ at -1.0 V vs. reversible hydrogen electrode, V_{RHE}), while Co-NC showed a favorable HER activity ($>58\ mA\,cm^{-2}$ at $-1.0\ V_{RHE}$). Inspired by this observation, the single-atom catalysts engaging both Co and Ni with different Co/Ni ratios were proposed. The CoNi-NC catalysts maintained the high syngas yield (total current density $>74\ mA\,cm^{-2}$ at $-1.0\ V_{RHE}$) with tunable CO/H₂ ratios (0.23–2.26) suitable for subsequent thermocatalytic reactions. The findings in this study suggest that the choice of TM in a single-atom configuration can be an effective way of tuning the CO/H₂ ratios, thus facilitating the potential

[*] Q. He,[+] Prof. Dr. L. Song
National Synchrotron Radiation Laboratory, CAS Center for Excellence in Nanoscience, University of Science and Technology of China
Hefei, Anhui 230029 (China)
E-mail: song2012@ustc.edu.cn

Q. He,[+] Dr. J. H. Lee,[+] Y. Liu, Dr. Z. Xie, Prof. Dr. J. G. Chen
Department of Chemical Engineering, Columbia University
New York, NY 10027 (USA)
E-mail: jgchen@columbia.edu

Dr. D. Liu[+]
School of Materials Science and Engineering, Nanyang Technological University
Singapore 639798 (Singapore)

Dr. Z. Xie, Prof. Dr. J. G. Chen
Chemistry Division, Brookhaven National Laboratory
Upton, NY 11973 (USA)

Dr. S. Hwang
Center for Functional Nanomaterials, Brookhaven National Laboratory
Upton, NY 11973 (USA)

Prof. Dr. S. Kattel
Department of Physics, Florida A&M University
Tallahassee, FL 32307 (USA)
E-mail: shyam.kattel@famu.edu

[+] These authors contributed equally to this work.

📄 Supporting information and the ORCID identification number(s) for
ⓘD the author(s) of this article can be found under:
https://doi.org/10.1002/anie.201912719.

adaption of electrochemical CO_2RR to syngas-mediated thermocatalytic processes.

In this work, the N-doped carbon supported single-atom catalysts were synthesized with the method reported previously.[6] In brief, glucose and dicyandiamide were well-mixed with TM-containing salts in deionized water, followed by evaporating the excess solvent. Then, the obtained powder precursors were annealed at 900°C to obtain the Co-NC, Ni-NC, and CoNi-NC catalysts. For a control sample, TM-free catalyst was synthesized (denoted as NC) with a similar method. Inductively coupled plasma-atomic emission spectroscopy (ICP-AES) measurements were used to analyze the metal contents (Supporting Information, Table S1) and confirmed that all of the samples have similar metal concentrations (ca. 1.2 wt.%).

The X-ray diffraction (XRD) pattern of CoNi-NC shows a peak around 26° corresponding to the (002) peak of the graphitic array (Figure 1a). Its broad peak profile reflects the disordered graphitic stacking along the c-axis and consequently high porosity, which thus helps the isolation of TM on the NC support. This is also in good agreement with the absence of obvious peak of TMs in the XRD profile. A series of catalysts including Co-NC, Ni-NC, and CoNi-NC shows similar XRD profiles (Supporting Information, Figure S1). High-resolution scanning transmission electron microscopy (STEM) image also displays an isolated TM environment as shown in Figure 1b, and in Figures S2a, S3a in the Supporting Information. The brighter spots indicate the well-isolated TM atoms rather than cluster formation on the NC. Furthermore, the elemental mapping analyses verify the homogeneous distribution of TM over the NC substrate (Figure 1c, and Figures S2b, S3b in the Supporting Information).
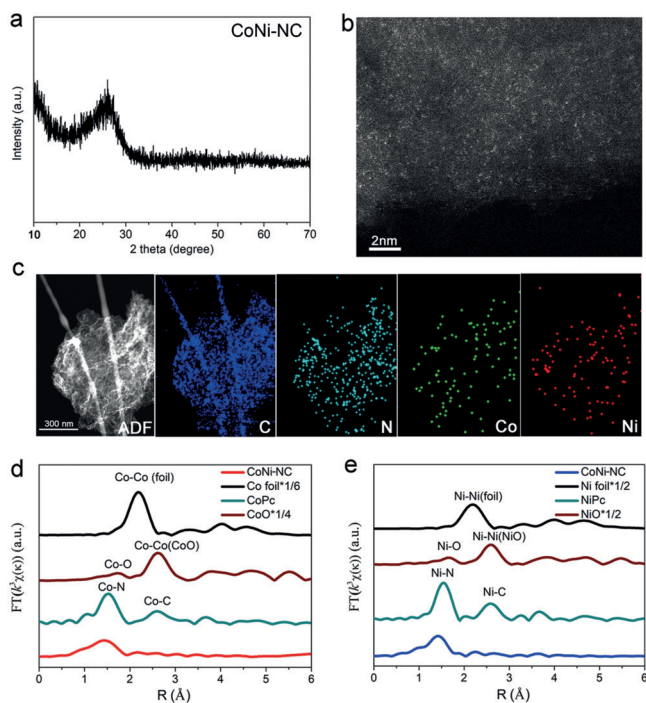
It is well-established that single TM atom cannot exist solely on carbonaceous support due to its high surface energy. As such, nitrogen incorporation into a carbon matrix can play an effective role in stabilizing single TM atom by the formation of the TM−N bond.[7] To verify the chemical information of CoNi-NC, Co-NC, and Ni-NC, X-ray photoelectron spectroscopy (XPS) analysis was carried out (Supporting Information, Figures S4–S6). XPS survey spectra show the coexistence of TM, N, and C. In the N 1s high-resolution spectra, all the catalysts exhibit four deconvoluted peaks at 398.2 eV (pyridinic-N), 399.7 eV (pyrrolic-N), 401.0 eV (graphitic-N), and 403.3 eV (oxidized-N). Pyridinic-N among these configurations was identified to be one of the dominant N species, which was attributed to the favorable TM−N bond formation.[8] Such a nitrogen configuration is consistent with the previous reports on similar single metal-NC catalysts and is also expected to partially oxidize TM through the electron transfer from TM to pyridinic-N.[9]

To explore the local physicochemical information around TM in TM-NC, X-ray absorption near-edge structure (XANES) and extended X-ray absorption fine structure (EXAFS) analyses were performed.[10] The XANES profiles of CoNi-NC at the Co and Ni K-edges reveal that the oxidation states of both Co and Ni are between 0 and 2+ (Supporting Information, Figure S7), implying both TMs are partially oxidized as a consequence of TM−N bond formation. For comparison, Co- and Ni-phthalocyanine (CoPc/NiPc) compounds were measured together due to their similar local structure around TM.[9] It is worth noting that CoNi-NC shows weakened X-ray absorption peaks at Co and Ni K-edges (dotted circle in Figure S7 in the Supporting Information), corresponding to the 1s→4p_z transition, than those in Co- and Ni-phthalocyanine (CoPc/NiPc). This transition can be used as a fingerprint for square-planar M-N_4 moieties and this intensity reduction thus confirms the distorted D_{4h} symmetry of TM atoms in CoNi-NC.[9a] The local structural information around TM can be further confirmed from the EXAFS analysis. The Fourier-transformed (FT) k^3-weighted EXAFS profiles of CoNi-NC at both Co and Ni K-edges show one notable peak around circa 1.4 Å, corresponding to the TM−N bond with a negligible TM–TM interaction in higher R-regions. The peak positions are similar to those of CoPc/NiPc and shorter than those of the TM−O bond in CoO/NiO (Figures 1d, e), suggesting that single-atom structure of TM is achieved owing to the presence of metal-N configuration. The Co-NC and Ni-NC are characterized by a similar local structure as CoNi-NC, as suggested by their similar XANES and EXAFS profiles (Supporting Information, Figures S8, S9). From the combined structural analyses using XRD, STEM, XPS, and XAFS characterization, all the TM-NC samples in this study most likely possess the single-atom configuration with pyridinic-N coordination.

The electrochemical activity of a series of TM-NC samples toward the CO_2RR was evaluated by using the chronoamperometry method in high-purity CO_2-saturated 0.5 M potassium bicarbonate ($KHCO_3$) aqueous solution with vigorous stirring. The obtained gaseous products were quantified by gas chromatography (GC, see the details in Experimental Sec-

Figure 1. Structural analysis of CoNi-NC. a) XRD pattern. b) HAADF-STEM image. c) Elemental mapping. d, e) Fourier-transformed (FT) k^3-weighted EXAFS profiles at d) Co and e) Ni K-edge.

tion). To distinguish the TM single atom from the typical TM nanoparticle (denoted as Co/NC and Ni/NC, in Figure S10 in the Supporting Information), these catalysts were also tested under the same condition. The representative chronoamperometric current densities at given potentials are presented in Figure S11 in the Supporting Information. All the samples exhibited CO and H_2 as the major gaseous products with the sum of their faradaic efficiency (FE) being near 100% within the potential range in this study.

However, it was revealed that the catalytic conversion of CO_2-to-CO was significantly affected by the TM choice. For the case of Co-NC (Supporting Information, Figure S12 a), FE(H_2) remained almost unchanged near 80% throughout the entire potentials with FE(CO) being near 20%, with the total current density increasing and reaching circa 72 mA cm^{-2} at -1.0 V$_{RHE}$ (Supporting Information, Figure S12 b). In contrast, Ni-NC was more selective to CO evolution over HER. With increasing overpotential, FE(CO) was higher than 90% from -0.5 V$_{RHE}$ to -0.9 V$_{RHE}$ and was 86% at -1.0 V$_{RHE}$ (Supporting Information, Figure S13 a). Moreover, Ni-NC showed high J(CO) values such as circa 12.1 mA cm^{-2} at -0.7 V$_{RHE}$ and circa 56 mA cm^{-2} at -1.0 V$_{RHE}$ (Supporting Information, Figure S13 b), which was better than Au NPs (7.9 mA cm^{-2} at -0.7 V$_{RHE}$) and immobilized Ag NPs (ca. 8.0 mA cm^{-2} at -1.0 V$_{RHE}$).[5c,11] In comparison, both Co/NC and Ni/NC nanoparticle and NC metal-free catalysts exhibited negligible CO_2RR activity (Supporting Information, Figures S14–S16). Thus, the high partial current densities observed in TM-NC can be attributed to the optimal utilization of TM due to the single-atom nature of TM.

In order to transform the obtained CO/H_2 into value-added chemicals by conventional thermochemical reactions, their ratio is important because it can control the product compositions.[12] Therefore, one can conclude that it is beneficial to balance CO_2RR activity and suitable CO/H_2 ratio (0.25–3.3) while increasing the overall CO/H_2 yield for a hybrid electro/thermocatalysis approach.[12] In this regard, both Co-NC and Ni-NC might not be a good choice because these catalysts would require an additional energy-consuming reactor that provides the missing component, either CO or H_2.

To this end, we evaluated CoNi-NC with an equal amount of Co and Ni as a representative bicomponent electrocatalyst. It was revealed that CoNi-NC produced a mixture of CO and H_2 with their FE ranging 45–55% within the potential range applied in the current study (Figure 2 a). Moreover, CoNi-NC still maintained the high total current densities (Figure 2 b and Figure S17 in the Supporting Information), indicating that the co-existence of Co and Ni did not interrupt the activity of each TM based single-atom catalyst. The CO/H_2 ratios (0.8–1.3, Figure 2 c) were in the suitable window of the typical thermochemical process such as Fischer–Tropsch and alcohol synthesis reactions, revealing the promising electrocatalytic properties of CoNi-NC for CO_2RR. Also, CoNi-NC exhibited excellent electrochemical performance (Figure 2 d), such a high total current density (ca. 51 mA cm^{-2}) and favorable FE(CO) of circa 53%, for 7 h consisting of the repeated 1 h electrolysis at -0.9 V$_{RHE}$, demonstrating promising stability
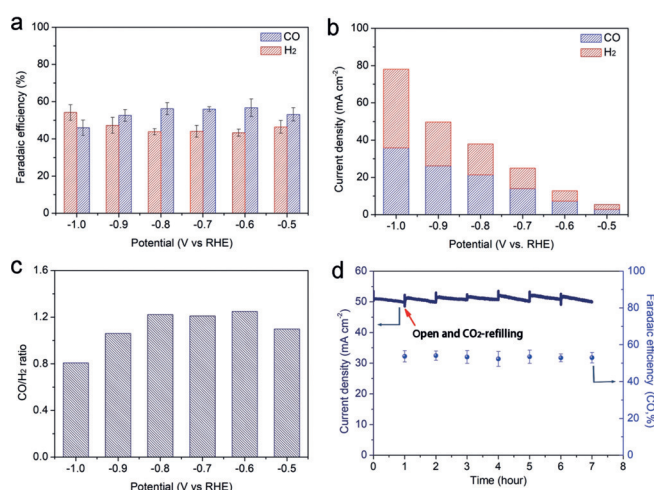
Figure 2. Electrochemical evaluation for CoNi-NC sample. a) Faradaic efficiencies for CO and H_2 evolution at different potentials. b) Partial current densities of CO and H_2 evolution at different potentials. c) Potential dependent CO/H_2 ratios. d) Long-term stability measured at -0.9 V$_{RHE}$.

essential for a hybrid electro/thermocatalytic system. Finally, the Faradaic efficiencies and current densities of the main samples at fixed potentials in a longer electrolysis period remained nearly constant, further illustrating the stability of the electrocatalysts (supporting Information, Figure S18).

CoNi-NC catalysts with different Co/Ni ratios (CoNi-NC-*x*, where *x* represents the precursor ratio of Co/Ni. Table S1 in the Supporting Information) were also tested under the same condition. All of these samples exhibited the stable chronoamperometry current density (Figures S19–S20). With increasing Co content, HER became more favorable over CO_2RR while maintaining high total current density, thus enhancing FE(H_2) (Supporting Information, Figures S21 and S22). These results imply that varying the Ni and Co ratio in CoNi-NC represents an opportunity of further tuning the CO/H_2 ratio without sacrificing the high syngas production rate.

Density functional theory (DFT) calculations were performed to gain insight into the activity and selectivity of Co-NC and Ni-NC catalysts for HER and CO_2RR. The binding energy of key reaction intermediates *H (for HER), and *HOCO and *CO (for CO_2RR) were calculated on Co-N$_4$ and Ni-N$_4$ centers embedded in a 4×4 graphene supercell (Figure 3 a), which have been proposed as potential active sites of Co-NC and Ni-NC catalysts, respectively.[14] Figures 3 a–f show the optimized structures of unit cells used in DFT calculations and the energetically most favorable adsorption configurations of the intermediates *H, *CO, and *HOCO on TM-N$_4$ (TM = Co, Ni) centers. It was found that the reaction intermediates bind at metal sites, indicating that the single metal atoms (Co and Ni) anchored in graphene plane by N coordination are active centers for catalysis. The DFT calculated binding energies in Figure 3 g show that the binding of the intermediates is significantly stronger on Co-N$_4$ compared to Ni-N$_4$. Thus, *HOCO formation, a key step/descriptor of CO_2RR,[15] is facilitated on Co sites compared to Ni sites (Supporting Information, Figure S23). However, the strong binding of *CO on Co-N$_4$ sites (BE $= -0.86$ eV) makes
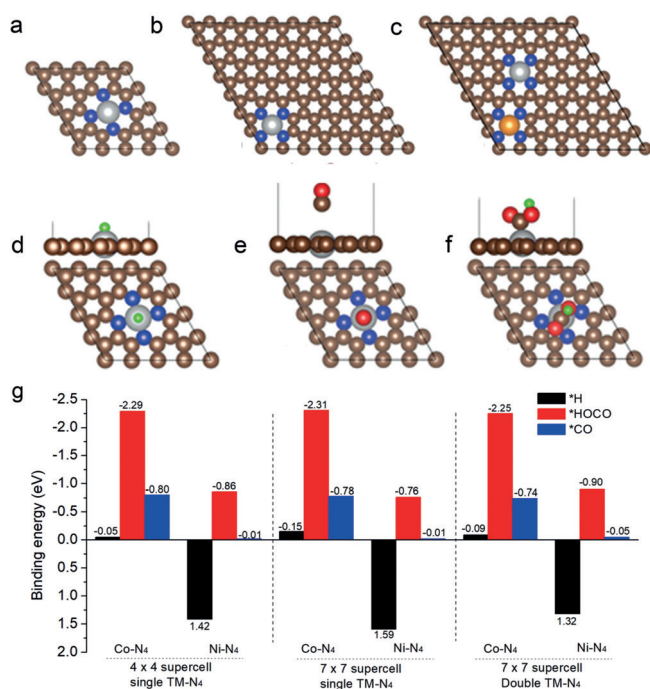
Figure 3. a–f) DFT optimized structures. a) Single Ni-N₄ on a 4×4 supercell. b) Single Ni-N₄ on a 7×7 supercell. c) Double Co-N₄ + Ni-N₄ on a 7×7 supercell. d) *H on Ni-N₄. e) *CO on Ni-N₄, and f) *HOCO on Ni-N₄. Ni: gray, Co: gold, C: brown, N: blue, O: red, and H: green. g) Calculated binding energies (in eV) on TM-N₄/C (TM = Co, Ni) centers.

its desorption, a potential independent step, the rate-limiting step of CO_2RR at all applied potentials on a Co-NC catalyst. On the Ni-N₄ sites, *HOCO formation is predicted to be the rate-limiting step based on the DFT calculated free energy diagrams at a potential $U = 0$ V (Supporting Information, Figure S23). The formation of *HOCO is a potential-dependent step and is expected to be facile at an applied external potential. Further, stabilization of *HOCO is expected due to the formation of hydrogen bonding (0–0.15 eV/bond) with water molecules at electrochemical conditions.[16] Finally, the desorption of *CO is predicted to proceed smoothly due to its weaker binding on the Ni-N₄ sites (BE = −0.01 eV). Thus, the DFT results predict that the CO_2RR is facilitated on Ni-N₄ compared to Co-N₄. The binding energy of *H has been identified as a descriptor of HER,[17] a competing reaction in CO_2RR. Figure 3g and Figure S23 (Supporting Information) show that the *H adsorption is stronger on Co-N₄ compared to Ni-N₄ and thus the HER should be more favorable on Co-N₄ compared to Ni-N₄. The stabilization of *HOCO under electrochemical conditions should favor the thermodynamics for CO_2RR compared to HER making the Ni-N₄/C sites selective to CO_2RR. In contrast, *HOCO stabilization should not play a role on the Co-N₄ sites for CO_2RR as *CO desorption is predicted to be the rate-limiting step. Overall, in agreement with the experimental measurements, the DFT results predict that Co-NC and Ni-NC should selectively promote the HER and CO_2RR, respectively.

Additional DFT calculations were performed to calculate the binding energies of the HER and CO_2RR intermediates using a 7×7 graphene supercell containing both Co and Ni, as shown in Figures 3b and c. It was noted from Figure 3g that the binding energies of the intermediates calculated on a 4×4 supercell are similar to those calculated on a 7×7 supercell with one (Figure 3b) and two TM-N₄ centers (Figure 3c). This suggests that the HER/CO_2RR selectivity of coexisting Co-N₄/Ni-N₄ sites, as shown in Figure 3c, is similar to that of single Co-N₄/Ni-N₄ sites shown in Figures 3a and 3b. Thus, consistent with the experimental results, the DFT calculations show that Co-N₄ and Ni-N₄ are predicted to be active sites for HER and CO_2RR, respectively, when both sites co-exist, which opens up the possibility of tuning the HER/CO_2RR selectivity by changing the Co/Ni ratio.

In order to further highlight the unique CO_2RR properties, a graph of $J(CO)$ versus $J(H_2)$ was constructed for all the TM-NC samples in this study (Supporting Information, Figure S24). Alongside these data points, we also included data points for other representative electrocatalysts to evaluate the syngas productivity of our samples (Supporting Information, Table S2).[5a,c,d,13] It can be seen that most of the catalysts, including Ni-NC in the current study, has been investigated to suppress HER. However, despite their high FE(CO), their low $J(CO)$ is still unsatisfactory to provide feedstock molecules to large scale thermochemical syntheses. CoNi-NC shows $J(CO)$ of 36 mA cm⁻² and CO/H_2 ratio of 0.81 at −1.0 V_{RHE}. Such values are remarkable because $J(CO)$ is comparable or even higher than those of the typical nanostructured catalysts, but is also capable of producing similar $J(H_2)$ at the same time.[5a,b,13] Moreover, the CO/H_2 ratio can be easily tunable by simply modifying the Co/Ni ratio in the CoNi-NC catalysts without sacrificing the high syngas yield (Supporting Information, Table S3).

In summary, we have investigated cost-effective TM-NC samples as CO_2RR electrocatalysts. All the catalysts exhibited high total current densities, which can be attributed to the single-atom configuration and the consequently optimal TM utilization. In order to tune the CO/H_2 ratios convenient for their utilization in thermochemical reactions, a series of CoNi-NC catalysts, where Co and Ni with different ratios coexisted in a single-atom configuration, were proposed to exhibit controllable CO/H_2 ratios while maintaining high total current densities. This work provides promising catalyst candidates to precious metal-based catalysts for high-yield syngas production with a tunable ratio of CO/H_2, demonstrating the feasibility for potential hybrid electro/thermocatalytic processes for CO_2RR.

Acknowledgements

Conflict of interest

The authors declare no conflict of interest.

[1] a) S. Xu, E. A. Carter, *Chem. Rev.* **2019**, *119*, 6631–6669; b) S. Lin, C. S. Diercks, Y.-B. Zhang, N. Kornienko, E. M. Nicolas, Y. Zhao, A. R. Paris, D. Kim, P. Yang, O. M. Yaghi, C. J. Chang, *Science* **2015**, *349*, 1208–1213.

[2] a) J. Qiao, Y. Liu, F. Hong, J. Zhang, *Chem. Soc. Rev.* **2014**, *43*, 631–675; b) P. Gao, S. Li, X. Bu, S. Dang, Z. Liu, H. Wang, L. Zhong, M. Qiu, C. Yang, J. Cai, W. Wei, Y. Sun, *Nat. Chem.* **2017**, *9*, 1019–1024; c) S. Gao, Y. Lin, X. Jiao, Y. Sun, Q. Luo, W. Zhang, D. Li, J. Yang, Y. Xie, *Nature* **2016**, *529*, 68–71; d) H. Rao, L. C. Schmidt, J. Bonin, M. Robert, *Nature* **2017**, *548*, 74–77.

[3] a) Y. Hori, *Mod. Aspects Electrochem.* **2008**, *42*, 89–189; b) B. M. Tackett, E. Gomez, J. G. Chen, *Nat. Catal.* **2019**, *2*, 381–386.

[4] C. Kim, F. Dionigi, V. Beerman, X. Wang, T. Moller, P. Strasser, *Adv. Mater.* **2019**, *31*, 18056175.

[5] a) J. H. Lee, S. Kattel, Z. Xie, B. M. Tackett, J. Wang, C.-J. Liu, J. G. Chen, *Adv. Funct. Mater.* **2018**, *28*, 1804762; b) W. Zhu, Y.-J Zhang, H. Zhang, H. Lv, Q. Li, R. Michalsky, A. A. Peterson, S. Sun, *J. Am. Chem. Soc.* **2014**, *136*, 16132–16135; c) C. Kim, H. S. Jeon, T. Eom, M. S. Jee, H. Kim, C. M. Friend, B. K. Min, Y. J. Hwang, *J. Am. Chem. Soc.* **2015**, *137*, 13844–13850; d) D. H. Won, H. Shin, J. Koh, J. Chung, H. S. Lee, H. Kim, S. I. Woo,

Angew. Chem. Int. Ed. **2016**, *55*, 9297–9300; *Angew. Chem.* **2016**, *128*, 9443–9446; e) H. Huang, H. Jia, Z. Liu, P. Gao, J. Zhao, Z. Luo, J. Yang, J. Zeng, *Angew. Chem. Int. Ed.* **2017**, *56*, 3594–3598; *Angew. Chem.* **2017**, *129*, 3648–3652.

[6] D. Liu, C. Wu, S. Chen, S. Ding, Y. Xie, C. Wang, T. Wang, Y. A. Haleem, Z. Rehman, Y. Sang, Q. Liu, X. Zheng, Y. Wang, B. Ge, H. Xu, L. Song, *Nano Res.* **2018**, *11*, 2217–2228.

[7] X.-F. Yang, A. Wang, B. Qiao, J. Li, J. Liu, T. Zhang, *Acc. Chem. Res.* **2013**, *46*, 1740–1748.

[8] S. Wang, Q. He, C. Wang, H. Jiang, C. Wu, S. Chen, G. Zhang, L. Song, *Small* **2018**, *14*, 1800128.

[9] a) H. B. Yang, S.-F. Hung, S. Liu, K. Yuan, S. Miao, L. Zhang, X. Huang, H.-Y. Wang, W. Cai, R. Chen, J. Gao, X. Yang, W. Chen, Y. Huang, H. M. Chen, C. M. Li, T. Zhang, B. Liu, *Nat. Energy* **2018**, *3*, 140–147; b) L. Cao, Q. Luo, W. Liu, Y. Lin, X. Liu, Y. Cao, W. Zhang, Y. Wu, J. Yang, T. Yao, S. Wei, *Nat. Catal.* **2019**, *2*, 134–141.

[10] K. Jiang, S. Siahrostami, T. Zheng, Y. Hu, S. Hwang, E. Stavitski, Y. Peng, J. Dynes, M. Gangisetty, D. Su, K. Attenkofer, H. Wang, *Energy Environ. Sci.* **2018**, *11*, 893–903.

[11] Z. Cao, S. B. Zacate, X. Sun, J. Liu, E. M. Hale, W. P. Carson, S. B. Tyndall, J. Xu, X. Liu, X. Liu, C. Song, J.-H. Luo, M.-J. Cheng, X. Wen, W. Liu, *Angew. Chem. Int. Ed.* **2018**, *57*, 12675–12679; *Angew. Chem.* **2018**, *130*, 12857–12861.

[12] M. B. Ross, Y. Li, P. D. Luna, D. Kim, E. H. Sargent, P. Yang, *Joule* **2019**, *3*, 257–264.

[13] W. Sheng, S. Kattel, S. Yao, B. Yan, Z. Liang, C. J. Hawxhurst, Q. Wu, J. G. Chen, *Energy Environ. Sci.* **2017**, *10*, 1180–1185.

[14] K. Jiang, S. Siahrostami, A. J. Akey, Y. Li, Z. Lu, J. Lattimer, Y. Hu, C. Stokes, M. Gangishetty, G. Chen, Y. Zhou, W. Hill, W.-B. Cai, D. Bell, K. Chan, J. K. Nørskov, Y. Cui, H. Wang, *Chem* **2017**, *3*, 950–960.

[15] J. T. Feaster, C. Shi, E. R. Cave, T. Hatsukade, D. N. Abram, K. P. Kuhl, C. Hahn, J. K. Nørskov, T. F. Jaramillo, *ACS Catal.* **2017**, *7*, 4822–4827.

[16] F. Calle-Vallejo, J. I. Martínez, J. Rossmeisl, *Phys. Chem. Chem. Phys.* **2011**, *13*, 15639–15643.

[17] J. K. Nørskov, T. Bligaard, A. Logadottir, J. R. Kitchin, J. G. Chen, S. Pandelov, U. Stimming, *J. Electrochem. Soc.* **2005**, *152*, J23–J26.